Highly Concentrated LiTFSI-EC Electrolytes for Lithium Metal Batteries

Downloaded from: https://research.chalmers.se, 2025-12-05 04:39 UTC

Citation for the original published paper (version of record):
Nilsson, V., Kotronia, A., Lacey, M. et al (2020). Highly Concentrated LiTFSI-EC Electrolytes for Lithium Metal Batteries. ACS Applied Energy Materials, 3(1): 200-207.
http://dx.doi.org/10.1021/acsaem.9b01203

N.B. When citing this work, cite the original published paper.

research.chalmers.se offers the possibility of retrieving research publications produced at Chalmers University of Technology. It covers all kind of research output: articles, dissertations, conference papers, reports etc. since 2004. research.chalmers.se is administrated and maintained by Chalmers Library

(article starts on next page)

This article is made available for a limited time sponsored by ACS under the ACS Free to Read License, which permits copying and redistribution of the article for non-commercial scholarly purposes.

ACS APPLIED ENERGY MATERIALS

Article

Cite This: ACS Appl. Energy Mater. 2020, 3, 200−207

www.acsaem.org

Highly Concentrated LiTFSI−EC Electrolytes for Lithium Metal Batteries

Viktor Nilsson,*[,†,‡,§] Antonia Kotronia,[‡] Matthew Lacey,[‡] Kristina Edström,[‡,§] and Patrik Johansson[†,§]

[†]Department of Physics, Chalmers University of Technology, SE-412 96 Gothenburg, Sweden

[‡]Ångström Laboratory, Department of Chemistry, Uppsala University, Box 538, SE-751 21 Uppsala, Sweden

[§]CNRS FR 3104, Hub de l'Energie, ALISTORE—European Research Institute, 15 Rue Baudelocque, 80039 Amiens Cedex, France

Supporting Information

ABSTRACT: Concentrated electrolytes have the potential to increase the stability for batteries with lithium metal anodes. In this study, liquid electrolytes were created by mixing ethylene carbonate (EC), a solid at room temperature, with a high concentration of LiTFSI salt. The binary LiTFSI−EC highly concentrated electrolytes have the benefit of extremely low volatility as compared to conventional organic electrolytes and also allow for cycling vs Li metal anodes. Using a LiTFSI−EC electrolyte with molar ratio 1:6, the Coulombic efficiency for Li plating/stripping on Cu is 97% at a current density of 1 mA cm^{-2} with a 2 mAh cm^{-2} capacity, pointing to a practically useful performance. In a full cell setup using a commercial $LiFePO_4$ (LFP) cathode, the efficiency is maintained, proving compatibility. In comparison to other carbonate-based electrolytes, there is less accumulation of decomposition products on the surface of a cycled Li film, which in part explains the improved cycle life. In all, this electrolyte system shows promise in terms of electrochemical stability and may allow for safe Li metal batteries due to the inherent physical stability.

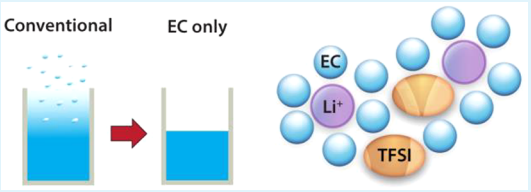

KEYWORDS: *highly concentrated electrolyte, Li metal anode, ethylene carbonate, anode free, safe electrolyte*

1. INTRODUCTION

Lithium metal has a theoretical capacity of 3860 mAh g^{-1}, ca. 10 times that of the graphite applied as anode material in current lithium-ion batteries (LIBs). It also has the lowest electrochemical potential of all metals and is thus seen as the ultimate lithium battery anode.[1] Rechargeable Li metal batteries were commercialized already in the 1970s, but withdrawn from the market in 1989 after the discovery of major safety issues.[2] The main problem was and still is the growth of Li dendrites ultimately penetrating the separator, resulting in short circuits and, in the worst cases, fires.[2] Moreover, after the commercialization of the LIB, using intercalation anodes such as graphite, most research activities on Li metal batteries were suppressed, but because the LIB technology today is quite mature, the appeal of high energy density batteries has caused a renewed interest in Li metal anodes.[1]

The highly reactive Li metal surface easily causes reduction of most electrolytes upon contact and ideally a solid electrolyte interphase (SEI) is formed, preventing continuous electrolyte degradation.[3] Unfortunately this is not enough for lithium electrodes—cycled lithium does not (re)deposit as a smooth and homogeneous film underneath the SEI, and the electrolyte is therefore repeatedly exposed to fresh metallic lithium.[4] When a Li metal battery is cycled, the successive stripping and plating of Li leads to the appearance of a rough surface layer irrespective of the smoothness of the initial Li metal foil.[5] This causes consumption of both Li metal and electrolyte, which therefore both have to be provided in excess, lowering the practical energy density of the electrochemical cell.[6] Furthermore, over time, the decomposition products may form a thick film with high resistance, limiting the performance and ultimately the life length of the cell.[7] Apart from strategies directly modifying the anodes such as composites[8] and surface coatings,[9] the electrolyte composition, whether liquid or solid, is the main variable.

The nature of the SEI and the obtained Coulombic efficiency (CE) are two of the most important factors determining the Li-plating morphology,[10] and they are both affected by the choice of electrolyte. A high CE indicates that less side reactions are occurring between Li and the electrolyte, while a thin and flexible SEI allows the Li to be plated underneath without cracking, which minimizes the surface area and also increases the CE.[11]

One of the most widely used electrolytes in the Li−S battery research field, a concept which relies on a Li metal anode, is composed of lithium bis(trifluoromethanesulfonyl)imide (LiTFSI) in a mixture of 1,3-dioxolane (DOL) and 1,2-dimethoxyethane (DME) with lithium nitrate ($LiNO_3$) as an additive to improve the CE.[12] A significant drawback of these

Received: June 17, 2019
Accepted: December 4, 2019
Published: December 4, 2019

Downloaded via CHALMERS UNIV OF TECHNOLOGY on May 20, 2020 at 12:31:50 (UTC).
See https://pubs.acs.org/sharingguidelines for options on how to legitimately share published articles.

© 2019 American Chemical Society

DOI: 10.1021/acsaem.9b01203
ACS Appl. Energy Mater. 2020, 3, 200−207

ether-based electrolytes for Li metal batteries is the poor oxidation stability[13,14] limiting compatibility with even moderate voltage LIB cathodes.

A promising alternative class of electrolytes for use with Li metal anodes is highly concentrated electrolytes (HCEs).[15,16] One of the early reports on HCEs described the suppression of Li dendrite formation using lithium bis(pentafluoroethanesulfonyl)imide (LiBETI) in propylene carbonate (PC).[17] More recently, HCEs of lithium bis(fluorosulfonyl)imide (LiFSI) in DME showed stable cycling of Li metal at high rates.[18] HCEs form SEIs significantly richer in inorganic salt decomposition products at the expense of organic components originating from the solvents, a natural consequence of their compositions.[17,19] Moreover, the bulk properties of HCEs, such as Li^+ diffusivity, concentration,[20] and transference number,[21] influence the interaction with the Li metal electrode beneficially.

High concentrations of LiTFSI in ethylene carbonate (EC) were introduced as an HCE concept by McOwen et al. in their study aiming to prevent Al corrosion, commonly occurring in LiTFSI-based electrolytes above ca. 3.5−4 V vs Li^+/Li.[22] They presented a phase diagram over liquidus, solidus, and glass transition temperatures over a range of LiTFSI mole fractions in EC, from 0 to 0.5 (i.e., up to 1:1 LiTFSI:EC). From this phase diagram, two compositions are of special interest: the eutectic point at 1:6 and the region at 1:2 LiTFSI:EC, where crystallization is suppressed. Avoiding volatile cosolvents such as DME or diethyl carbonate (DEC) should result in an inherently safer electrolyte. Although LiFSI has been popular in HCEs lately, we still believe LiTFSI has its merits as an electrolyte salt.[23] LiTFSI is also cheaper and more readily available with high purity.[24] Recently, concentrated multisalt electrolytes based on LiFSI and LiTFSI have been tested in studies similar to this, with demanding conditions using low or zero Li excess in full cells.[25,26]

In order to determine if LiTFSI−EC HCEs are compatible and cycle with Li metal anodes, we here compare two compositions (1:6 and 1:2) to three reference electrolytes: an LiTFSI-analogue to LIB electrolytes using EC and DEC, an "Li−S battery electrolyte" as a benchmark for Li metal plating, and a direct substitution of EC with PC. PC has physical properties similar to those of EC, e.g., viscosity and vapor pressure, but the electrochemical reduction behavior differs: EC has a clear reduction peak at 1.36 V vs Li^+/Li, while PC is reduced without any clearly defined peak in the range of 1.0−1.6 V.[28] Furthermore, EC is known to form far better SEIs on graphite[29] and cycle better vs Li metal.[30] By employing these comparisons, we hope to show that LiTFSI−EC HCEs are a good starting point when formulating liquid electrolytes for Li metal batteries.

2. EXPERIMENTAL SECTION

2.1. Materials. The salts lithium bis(trifluoromethanesulfonyl)-imide (LiTFSI, Solvionic, 99.9%, <20 ppm H_2O) and lithium hexafluorophosphate ($LiPF_6$, Sigma-Aldrich, 99.99%) were used as received, while lithium nitrate ($LiNO_3$, Sigma-Aldrich, 99.99%) was dried under vacuum at 120 °C overnight. The electrolyte solvents were of anhydrous grade from Sigma-Aldrich with the following purities: ethylene carbonate (EC), 99%; propylene carbonate (PC), 99.7%; diethyl carbonate (DEC), 99%; 1,2-dimethoxyethane (DME), 99.5%; 1,3-dioxolane (DOL), 99.8% with 75 ppm BHT, respectively. With the exception of the already dry EC, the solvents were dried over 3 Å molecular sieves overnight and subsequently filtered using 0.45 μm PTFE syringe filters. All handling of the salts and solvents took place in an Ar-filled glovebox (H_2O < 1 ppm; O_2 < 1 ppm).

Electrodes were cut from foils: thick Li (Cyprus Foote Mineral, 125 μm), thin Li (Rockwood Lithium, 30 μm), lithium iron phosphate on Al (LFP, Custom Cells, 3.5 mAh cm^{-2}, 160 μm, 61% porosity), and Cu (Goodfellow, 20 μm, >99.9%). The surface oxide on the Cu foil was removed by etching in nitric acid (HNO_3, VWR, 68%) diluted 1:2 (v/v) with distilled water. When Cu dissolution was observed evenly across the surface, the etching was stopped by washing the electrodes with distilled water, followed by ethanol (Solveco, 99.5%) before immediate transfer to an Ar-filled glovebox.

Separators were cut from Solupor 3P07A single-layer polyethylene membranes (Lydall, 20 μm, 83% porosity, Supporting Information Figure S1) and from Whatman GF/A glass fiber filters (GE Life Sciences, 0.26 mm). Both were dried under vacuum at 60 °C for at least 4 h.

2.2. Electrolytes. Molten EC was mixed with LiTFSI by magnetic stirring overnight at 50 °C to obtain the electrolytes 1:6 LiTFSI:EC and 1:2 LiTFSI:EC (molar ratios). This corresponds to 1.86 and 3.6 M, respectively, as calculated from measured densities at 20 °C. The 1:6 LiTFSI:PC (1.53 M at 20 °C), 1 M LiTFSI in 1:1 EC:DEC (v/v), and 1 M LiTFSI + 0.2 M $LiNO_3$ in 1:1 DOL:DME (v/v) electrolytes were prepared by magnetic stirring overnight at 20 °C. The two latter, specified by molarity (as opposed to molar ratio), were mixed in volumetric flasks, while the HCEs were weighed according to their mass fractions. The water content for all electrolytes was determined to <10 ppm using Karl Fischer coulometric titration inside the glovebox. For simplicity, the electrolytes are henceforth referred to as 6 EC, 2 EC, 6 PC, EC-DEC, and DOL-DME, respectively. A 1 M amount of $LiPF_6$ in 1:1 EC:DEC (v/v) was prepared just as EC-DEC and used for postmortem tests of LFP electrodes.

2.3. Physicochemical Characterization. The density and viscosity of each electrolyte were measured at every 10 °C from 10 to 80 °C using an Anton Paar DMA 4500 M density meter with a Lovis 2000 M rolling ball viscometer module.

The thermal stability was measured by dynamic thermogravimetric analysis (TGA). An Al crucible was filled with 70−90 μL of electrolyte and heated from 25 to 300 °C at a rate of 10 K min^{-1} using a 20 mL min^{-1} flow of N_2 purge gas in a Netzsch TG 209 F1 Iris instrument.

The melting point, defined as the minimum of the endothermic peak during heating, was determined by differential scanning calorimetry (DSC) using a TA Q2000 instrument. An Al crucible with ca. 25 mg of electrolyte was filled and sealed inside an Ar-filled glovebox. Two cycles were run with cooling to −80 °C followed by heating to +80 °C at a rate of 5 °C min^{-1} and with an automatic equilibration of ca. 1 min at the end points.

The ionic conductivity was measured by electrochemical impedance spectroscopy using a Novocontrol Concept 80 equipment. Coin cells were filled with electrolyte in an Ar-filled glovebox, using stainless steel (SS) electrodes and a 1 mm thick PTFE ring with an 8.2 mm inner diameter defining the sample volume. The cell impedance was measured at every 10 °C from −60 to 80 °C after 15 min thermal equilibration at each temperature, during both cooling and heating sequences after initial cooling to −60 °C. A 10 mV_{RMS} sinusoidal perturbation was applied from 133 mHz to 10 MHz, and the real part of the ionic conductivity was obtained from the high-frequency plateaus, typically at 133 kHz.

2.4. Electrochemical Tests. Coin cells, unless otherwise noted, Ni-plated SS 2025 cases with a 0.5 mm spacer disk and a wave spring, were assembled in an Ar-filled glovebox (H_2O < 2 ppm; O_2 < 5 ppm). The cells were then kept in an oven at ca. 65 °C for 1 h to assist wetting of the separators and LFP electrodes prior to ca. 20−40 h rest at room temperature. In some tests, more than one separator was used: the Solupor acts as a barrier toward dendrite growth, while the Whatman increases the stack pressure and distributes it more evenly across the electrodes. The latter separator also holds an excess of electrolyte, reveals dendrite penetration as dark deposits in the otherwise white/transparent material, and separates the degradation

DOI: 10.1021/acsaem.9b01203
ACS Appl. Energy Mater. 2020, 3, 200−207

at the anode from that at the cathode. Two cells of each kind were tested.

All tests used a constant current density of 1 mA cm^{-2}, large enough to be of practical relevance and to clearly discriminate between the different electrolytes. Cycling stability was first tested using symmetric Li metal cells, Li|Solupor|Whatman|Solupor|Li, with 16 mm o.d. electrodes, 17 mm o.d. separators, and 75 μL of electrolyte. The CE of Li plating on Cu was tested in Cu|Solupor|Whatman|Li cells, using 16 mm o.d. separators and Cu, 15 mm o.d. Li, and 70 μL of electrolyte (2032 cases; 1 mm spacer). The CE was calculated as the ratio of capacities, $Q_{stripped}/Q_{plated}$, where a 15 min hold at a cell voltage of 1 V terminated each cycle (Figure S6b). A capacity of 2 mAh cm^{-2} was used for all cells above.

Compatibility with the cathode material and Li plating efficiency were simultaneously tested in zero excess Li cells, Cu|Solupor|LFP, using 10 mm o.d. electrodes and 17 mm o.d. separators with 25 μL of electrolyte and cycled between cell voltages of 2.4–4.0 V. As a proof-of-concept the 6 EC HCE was tested in full Li metal cells, Li|Solupor|LFP, using 15 mm o.d. and 30 μm of thin Li, 13 mm o.d. LFP, 17 mm o.d. separators, and 20 μL of electrolyte. The cells were conditioned for one cycle at 0.1 mA cm^{-2} and then cycled at 1 mA cm^{-2} (C/3.5) between 3.1–3.7 V. For postmortem capacity tests the LFP electrodes were rinsed with dimethyl carbonate (DMC, Sigma-Aldrich, anhydrous, 99%), whereafter 1 M $LiPF_6$ in 1:1 EC:DEC (v/v; Solvionic, 99.9%) was used as the electrolyte.

2.5. Surface Characterization. Scanning electron microscopy (SEM) was used to investigate the morphology of Li deposited from the different electrolytes. To improve reproducibility and avoid local variations in morphology, etched Cu was used as substrate rather than Li foil. The Cu electrodes in Cu|Solupor|Whatman|Li cells were subjected to four plating/stripping cycles followed by a plating stage, all with a capacity of 2 mAh cm^{-2} at 1 mA cm^{-2}. The cells were disassembled in an Ar-filled glovebox, and subsequently the Li-coated Cu electrodes were rinsed with DMC, torn apart with tweezers to expose the cross-section, and transferred to the SEM in an airtight transfer chamber. For the best reproduction of the morphology and less disturbance by sample charging, the off-axis secondary electron detector (HE-SE2) was used in the microscope (Zeiss Merlin, 3 kV, 100 pA, WD ≈ 6 mm).

3. RESULTS AND DISCUSSION

The main focus of this study lies in understanding the behavior of these specific HCEs at the Li metal electrodes, but to set the stage some physicochemical properties are first investigated. The electrolytes are then tested electrochemically in a range of cell setups, together with investigations of the Li metal surface morphology. Finally, full Li metal cells with a low excess of both Li and electrolyte are tested as proof-of-concept and a step toward a practically relevant cell.

3.1. Physicochemical Properties. First, to show the stark difference between electrolytes with volatile solvents (DEC, DOL, and DME) and nonvolatile solvents (EC and PC), a dynamic TGA scan was run (Figure 1). The DOL and DME solvents both evaporate quickly already at room temperature and are almost gone when the material reaches 100 °C. Similarly, in EC-DEC the DEC starts evaporating at room temperature, accelerating at 75 °C, followed by a small plateau before the EC evaporation at 150 °C. The 2 EC, 6 EC, and 6 PC electrolytes are stable to above 100 °C, closely following pure EC up to 150 °C where the evaporation accelerates for all. This shows that the low vapor pressure of 6 EC is mainly inherited from the solvent and not an HCE effect. The less steep slope for 2 EC is a combined effect of the lower amount of solvent in the sample with total mass on the *y*-axis and slower kinetics. As EC evaporates from the 6 EC solution, the concentration increases which slows down the evaporation rate, and at the 300 °C test end point there is a 38.8% residual,

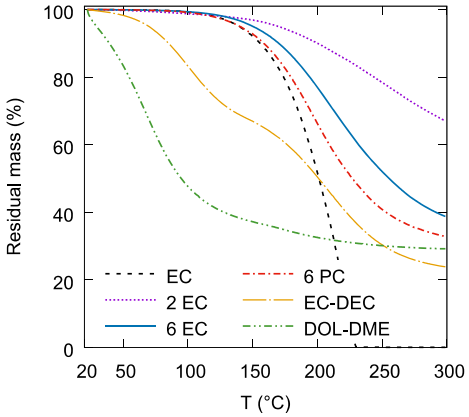

Figure 1. Thermogravimetric scans of pure EC and the electrolytes.

slightly above the initial LiTFSI mass of 35.2%. This residual consists of LiTFSI, EC, and possibly some decomposition products. LiTFSI in EC-PC electrolytes is known from literature to be stable at >300 °C in the absence of electrode materials,[31] justifying the assumption that mainly evaporation takes place here. The low volatility is beneficial for cell assembly as the time from filling to sealing becomes less crucial, there is less solvent exposure for workers, and there is a lower risk of combustible fumes escaping the cells. This safety aspect is further highlighted by the large difference in flash points: DOL and DME at −3 °C vs EC at 143 °C.[32−34]

The high electrolyte densities (Table 1) are primarily a result of the heavy anion (M_{TFSI} = 280 g mol^{-1}) and high

Table 1. Electrolyte Densities at 25 °C Interpolated from the Full Data in Table S1 (Errors, ≤±0.01 g cm^{-3})

	2 EC	6 EC	6 PC	EC-DEC	DOL-DME
ρ (g cm^{-3})	1.66	1.51	1.37	1.28	1.14

solvent density (ρ_{EC} = 1.32 g cm^{-3}) but are, of course, further increased by the very high salt concentrations. This has a negative effect on the resulting cell energy density, and likely also materials cost, as compared to LIB electrolytes using a lower concentration of $LiPF_6$ salt; 1 L of the 6 EC electrolyte contains 530 g of LiTFSI, while 1 L of a standard LIB electrolyte contains ca. 152 g of $LiPF_6$.

Turning to the electrolyte viscosities, these vary significantly between the electrolytes (Figure 2a). Sample 2 EC is extremely viscous, akin to liquid honey, which makes it difficult to dose into cells and results in slow wetting of electrodes and separators. As observed for other HCEs, the viscosity increase is due to incomplete solvation and strong ion−ion interactions.[15] The 6 EC and 6 PC electrolytes have viscosities of 20–30 mPa s at 20 °C, and hence, while still significantly higher than EC-DEC at 6 mPa s and DOL-DME at 2 mPa s, these electrolytes are all easy to handle. As a comparison, milk and full-fat cream have viscosities of ca. 3 and 30 mPa s, respectively.[35]

The ability to wet separators depends to a large extent on the viscosity but also on the lipophilicity of the electrolytes and separators. That the selection of separator is critical is evident from the complete inability of the HCEs to wet polypropylene Celgard 2400 (not shown). The Solupor separator is easily wet by 6 PC and EC-DEC and instantly wet by DOL-DME. In contrast, 6 EC does not wet the Solupor separator during

DOI: 10.1021/acsaem.9b01203
ACS Appl. Energy Mater. 2020, 3, 200−207

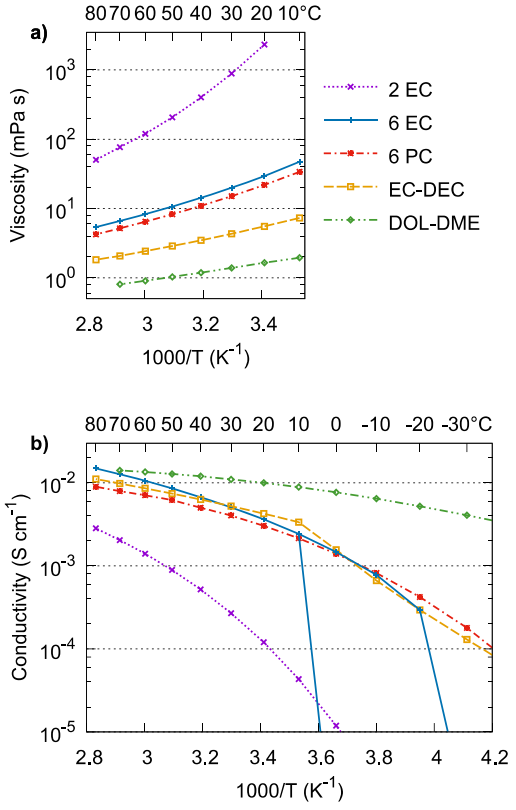

Figure 2. (a) Viscosities and (b) ion conductivities of the electrolytes. Full data in Tables S1a and S2b. Estimated errors in viscosity < 3% and conductivity < 13%.

assembly, but after heating, which accelerates wetting, and rest, the cells work consistently at rates of 1 mA cm^{-2} with homogeneous Li plating, and with separators found completely wet upon disassembly. In all electrolytes, the Solupor was easily removed from the Li surface after cycling and kept the black degradation products out of the fiberglass, showing that they prevented Li growth through the separator.

The ion conductivities (Figure 2b) are inversely correlated to the viscosity with the exception of 6 EC, which has a conductivity similar to that of the EC-DEC, despite a much higher viscosity. The conductivities at each equilibrated temperature are the same for cooling as heating, except for 6 EC. When cooling 6 EC, the ionic conductivity decreases smoothly until −20 °C, where the material likely crystallizes during cooling to −30 °C, observed as a sudden large drop in conductivity. When heating from 0 to 10 °C, this is recovered, which suggests that the electrolyte was supercooled between 10 and −20 °C. The conductivity curve for EC-DEC shows no discontinuity but a sudden change of slope between 0 and 10 °C, which suggests phase separation and partial crystallization since the conductivity keeps decreasing smoothly after the initial drop. The crystallization of both of these materials is also inferred from the exothermal events in the DSC traces, with melting points of 3 °C for 6 EC and 6 °C for EC-DEC (Figure S2). The melting point of 6 EC just above 0 °C agrees well with the literature.[22]

3.2. Electrochemical Properties. Starting with 2 EC the test using a current density of 0.1 mA cm^{-2} allowed cycling, but 1 mA cm^{-2} resulted in a cell polarization prohibitively high (Figure S3). This is most likely a consequence of the low electrolyte ionic conductivity and poor separator wetting, and the 2 EC electrolyte was discarded from further testing.

3.2.1. Symmetric Cells. Symmetric Li cells were cycled galvanostatically, and the cells with 6 PC and EC-DEC consistently failed early and also had a gradually increasing polarization (Figure 3a). In contrast, both 6 EC and DOL-DME have cells resulting in more erratic polarization and the time to failure varies substantially, suggesting different failure modes. The asymmetry of the polarization is likely a consequence of the cycling scheme, where one electrode starts

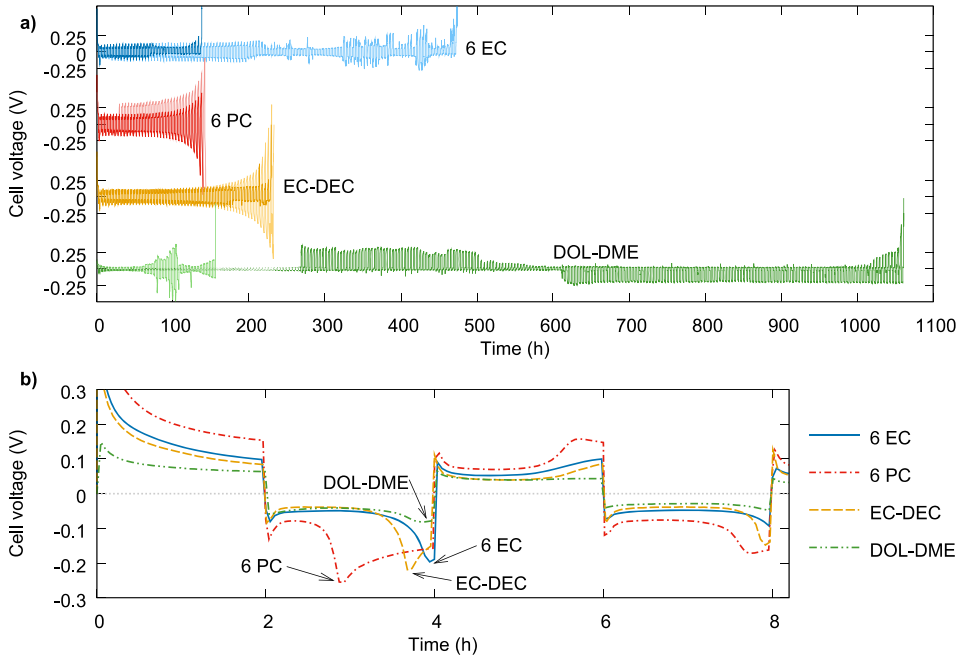

Figure 3. (a) Symmetric Li cells cycled at 1 mA cm^{-2} with lighter color behind for the duplicate cells, and (b) the first two cycles for one cell of each electrolyte.

DOI: 10.1021/acsaem.9b01203
ACS Appl. Energy Mater. 2020, 3, 200−207

as a substrate for Li deposition while the other starts with Li pitting. This asymmetry is visually observed through unbalanced degradation of the two Li electrodes.

The overpotential, which depends on both interfacial and bulk resistance, is highest for 6 PC followed by 6 EC, EC-DEC, and DOL-DME (Figure 3b). This correlates with the conductivities at 20 °C, and since a thick Whatman separator was used, the bulk resistance should contribute significantly. The peaks at the beginning and end of the cycles are characteristic and are due to a combination of nucleation, dendrite stripping, and bulk stripping.[36] A long plateau before a rise in potential indicates that a larger fraction of the deposited Li can be recovered before pitting of the bulk Li foil.[36] Judging, e.g., by the peaks at 3−4 h, the order of plating efficiency is 6 PC < EC-DEC < 6 EC ≈ DOL-DME. For DOL-DME, the peaks can barely be seen, which indicates a more homogeneous stripping and low activation energy for nucleation, in agreement with the literature.[36]

3.2.2. Coulombic Efficiency. For a more direct quantitative comparison of Li metal cycling stability in the electrolytes,[37] the CE was determined for two cells, in good agreement, for each choice of electrolyte and for each cycle of Li plating/stripping on a Cu substrate (Figure 4). The average CEs over

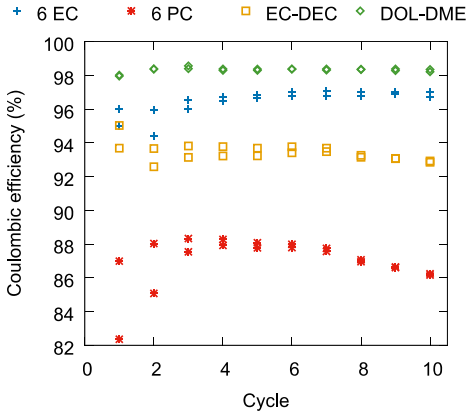

Figure 4. CE of Li plating on Cu with a current density of 1 mA cm^{-2} and a capacity of 2 mAh cm^{-2}. Each electrolyte is tested in two individual cells, all shown. Corresponding voltage profiles in Figure S6.

the 10 first cycles were as follows: DOL-DME, 98.3%; 6 EC, 96.5%; EC-DEC, 93.4%; and 6 PC, 87.1%; which is qualitatively consistent with the ordering of the symmetric cells above. Note that the specific values of the CEs depend strongly on the test conditions; our results are in reasonable agreement with, e.g., those of Qian et al.,[27] where a lower capacity of 0.5 mAh cm^{-2} is used for the CE test.

$LiNO_3$ is crucial for Li metal cycling in DOL-DME; without the additive the CE was within the range 10−60% (Figure S4). The EC-DEC electrolyte was tested in place of a dilute LiTFSI-EC electrolyte since the latter is solid at room temperature. Hypothetically, the stabilizing properties from EC could be maintained while lowering the viscosity compared to 6 EC. However, the measured performance is very poor, which agrees with the literature where DEC as a cosolvent had a detrimental effect on cycle life in both EC- and PC-based electrolytes.[30] Furthermore, the formation of an SEI rich in LiF, known to improve the Li morphology,[38] is less likely in EC-DEC than in 6 EC, because of the lower salt concentration. However, the difference between 6 PC and 6 EC shows that the high concentration alone does not suffice to reach high cycling stability.

3.2.3. Morphology. One way to examine how the electrochemical differences are reflected in the Li morphology is using SEM. After a single Li deposition cycle on a Cu electrode, a comparison between 6 EC and 6 PC reveals only minor differences, with the former resulting in slightly larger Li features. To better match the electrochemical tests, however, the effect of repeated Li stripping/plating was studied using all four electrolytes, four full cycles, and examining the fifth cycle deposition.

The films deposited using the carbonate electrolytes all appear similar, with mossy top structures (Figure 5a) and Li films comprised of densely packed columns underneath leftover SEI from previous cycles (Figure 5b). The patterns on the top surfaces are imprints of the separator (Figure S1). The columnar morphology resembles what has been reported for $LiPF_6$−PC electrolytes.[39] The Li columns formed in 6 EC are ca. 1 μm wide, while the Li films formed in 6 PC and EC-DEC contain more sub-micrometer features. These columnar Li films are re-formed as dense films on the Cu substrate also in later cycles, indicating that the old SEI does not hinder access to the substrate but is instead forced outward from the electrode. For 6 PC (Figure 5d) and EC-DEC (Figure S7) individual layers of dead material are observed and an increasing polarization resulting from an accumulation of these layers is the most likely failure mode (Figure 3a). The dead material from 6 EC (Figure 5c) is thinner and does not seem to form layers. The amount of dead material should decrease with increasing CE, and furthermore, the wider Li columns in 6 EC lower the surface area of fresh Li exposed to electrolyte, which could contribute to the higher CE.

In stark contrast to the columnar structure, the ether-based DOL-DME results in films formed from Li globules with 1−6 μm o.d. Furthermore, the coverage of the Cu substrate is less dense, which together with the large globules indicates that growth on existing Li is energetically favored. This globular morphology is predominantly caused by the presence of $LiNO_3$, as a DOL-DME electrolyte without $LiNO_3$ behaves quite differently (Figure S5), in agreement with earlier observations.[40]

3.2.4. Zero Excess Full Cells. So far only the anode side has been considered; to probe how the electrolytes would fare in a full Li metal cell, zero excess full cells were used. These tests are very significant as they probe compatibility with the cathode material while still testing anode stability, revealing inefficiencies that are masked by the excess of Li when using Li metal anodes.[41] Additionally, using these cells with low electrolyte loading and thin separators gives more realistic conditions. Here cells with a nominal cathode capacity of 3.5 mAh cm^{-2} were cycled for 30 cycles (Figure 6a). The nominal capacity is only reached during the first charge (LFP delithiation) and is never fully recovered.

The cells using 6 PC lose all capacity within 20 cycles, while for all other electrolytes the remaining discharge capacities averaged over two cells after 30 cycles were as follows: EC-DEC, 8%; DOL-DME, 22%; and 6 EC, 41%. The overall highest capacity loss is observed in the first cycle and is largest for DOL-DME, where the first charge stage indicates severe electrolyte oxidation (Figure 6b). Overall, the results are similar to those reported for Cu|LFP cells in the literature.[26,27]

DOI: 10.1021/acsaem.9b01203
ACS Appl. Energy Mater. 2020, 3, 200−207

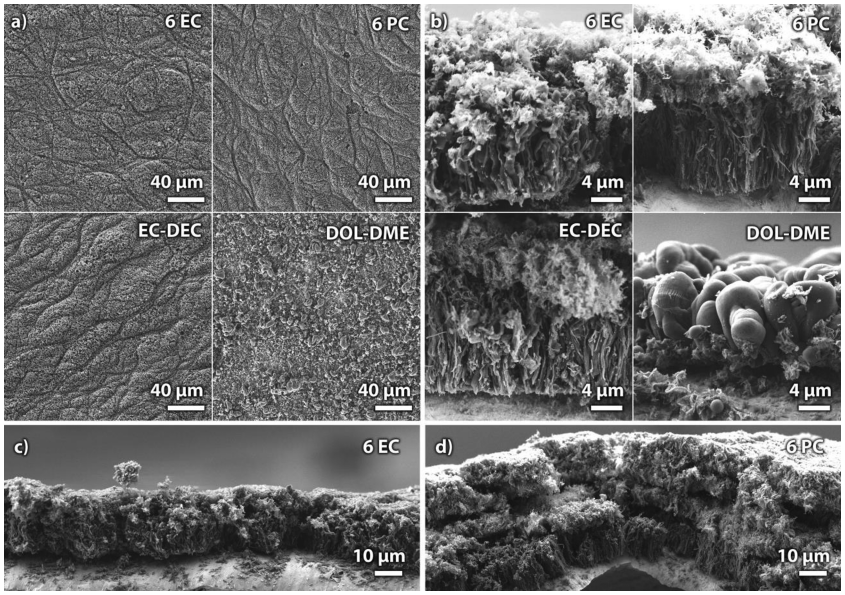

Figure 5. Film deposited on Cu after the fifth Li-plating step: (a) Top view; (b) side view of Li in torn cross-section; (c, d) overviews of cross-section. Full versions of panel b are shown in Figure S7.

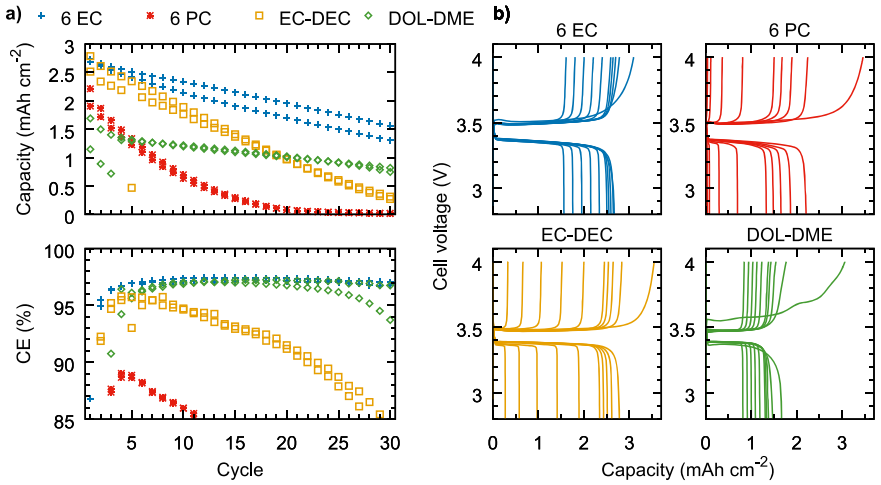

Figure 6. (a) Discharge capacities and CEs for CulSoluporlLFP cells (two cells/electrolyte). For 6 PC some data points are out of the ranges shown. (b) Charge and discharge voltage profiles for cycles 1−5, 10, 15, 20, 25, and 30 (one cell/electrolyte; see also Figure S8).

The cell to cell variation is significantly smaller than the effect of the electrolyte.

The CE was averaged over the 10 first cycles for comparison to the CulLi cells, where the best cell for each electrolyte was chosen to avoid the outliers in cycles 1−5 for DOL-DME and EC-DEC. The average CEs are as follows: 6 PC, 84.7%; DOL-DME, 90.4%; EC-DEC, 93.3%; and 6 EC, 95.9%. For the carbonate cells the CE is not significantly affected by the use of LFP, but for the DOL-DME electrolyte the CE drops from 98.3% in CulLi cells to 90.4% in CulLFP cells (94.3% excluding the first cycle). This is not surprising given the lower oxidation stability of ethers, resulting in a sloping voltage profile just below the upper cutoff, especially for the early cycles (Figure 6b). After the first cycles, the capacity fading rate for DOL-DME is lower as compared to 6 EC, which could be due to the lower capacity per cycle, following from the larger initial capacity drop.

To verify that the capacity loss was caused by electrolyte decomposition and loss of cyclable Li, and not by active material degradation, the LFP cathodes were tested in new cells with fresh Li and 1 M $LiPF_6$ in EC:DEC electrolyte (Figure S9). All recovered a capacity of >3.3 mAh cm^{-2}, higher than the first discharge capacity, and were thus intact.

3.2.5. Full Lithium Metal Cell. With 6 EC established as the best electrolyte it was further tested in full Li metal cells using a 30 μm Li foil—1.8× overcapacity vs the LFP cathode and thin enough to be of practical relevance.[42] A single Solupor separator with an electrolyte volume of 8.8 μL cm^{-2} was used resulting in an average CE for cycles 2−61 of 98.7%, which is limited by the cathode, and after 65 cycles the capacity and CE drop (Figure 7a). Compared to similar experiments where, as here, both the electrolyte volume and the Li foil thickness were limited,[43] the smooth onset of the capacity drop suggests that electrolyte depletion is a likely and significant failure mode. The larger growth of cell polarization (Figure 7b) as compared to the zero-excess cells may be attributed to the higher capacity per cycle and lower electrolyte volume. A duplicate cell

DOI: 10.1021/acsaem.9b01203
ACS Appl. Energy Mater. 2020, 3, 200−207

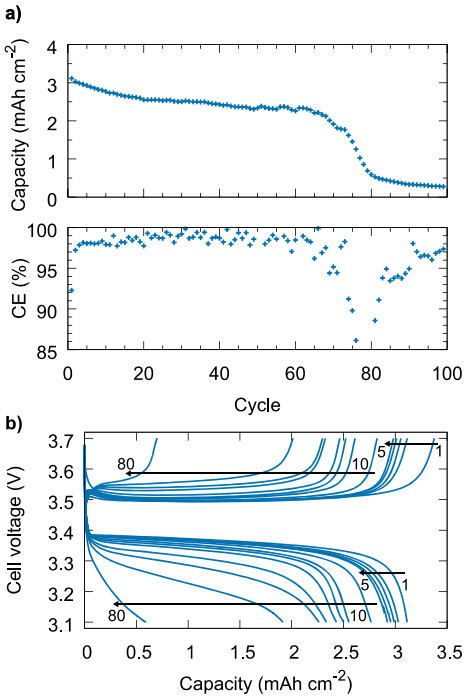

Figure 7. (a) Discharge capacities and CE for a LilLFP cell at 1 mA cm^{-2} and (b) voltage profiles, cycles 1−5 and every 10 cycles from 10 to 80.

showing similar behavior with slightly lower capacities and earlier failure is shown in Figure S10.

4. CONCLUSION

The highly concentrated 6 EC electrolyte offers a stability vs Li metal anodes close to that of the DOL-DME electrolyte, but with superior performance when paired with 4 V cathodes. Furthermore, the low volatility and the high flash point should lead to safer cells and could also allow for operation at elevated temperatures.

The outlook for further improvements is promising; very small fractions of volatile cosolvents such as DMC could be added to improve the electrochemical performance[30] and also separator wetting without necessarily compromising the safety benefits, cosalts such as $LiNO_3$ or $LiPF_6$ can be used to improve the stability—even millimolar concentrations of $LiNO_3$ can be beneficial,[44] or changing from LiTFSI to LiFSI.[18] Furthermore, to ease manufacturability of cells employing HCEs, a careful selection of the separators should be made, e.g., with polar surface groups and suitable porosities. Overall, the 6 EC HCE shows substantial promise as an electrolyte basis for further development toward the realization of fully functional Li metal cells.

■ ASSOCIATED CONTENT

Supporting Information

The Supporting Information is available free of charge at https://pubs.acs.org/doi/10.1021/acsaem.9b01203.

Additional and full versions of SEM images, DSC traces, SEM and electrochemical comparison of the impact of $LiNO_3$ in DOL-DME, tabulated ionic conductivities and viscosities, electrochemical data for duplicate cells, voltage profiles for CE test, and LFP electrode integrity test and polarization using 2 EC electrolyte (PDF)

■ AUTHOR INFORMATION

Corresponding Author

*E-mail: viktor.nilsson@chalmers.se.

ORCID

Viktor Nilsson: 0000-0002-3966-6219
Matthew Lacey: 0000-0002-0366-7228
Kristina Edström: 0000-0003-4440-2952
Patrik Johansson: 0000-0002-9907-117X

Notes

The authors declare no competing financial interest.

■ ACKNOWLEDGMENTS

We are grateful to the Swedish Energy Agency ("Batterifonden" Grant No. 39042-1) and Alistore-ERI for financial support to V.N. We also acknowledge the support from StandUp for Energy and several of Chalmers' Areas of Advance: Materials Science, Energy, and Transport.

■ REFERENCES

(1) Lin, D.; Liu, Y.; Cui, Y. Reviving the Lithium Metal Anode for High-Energy Batteries. *Nat. Nanotechnol.* **2017**, *12* (3), 194−206.
(2) Brandt, K. Historical Development of Secondary Lithium Batteries. *Solid State Ionics* **1994**, *69* (3), 173−183.
(3) Peled, E. The Electrochemical Behavior of Alkali and Alkaline Earth Metals in Nonaqueous Battery Systems—The Solid Electrolyte Interphase Model. *J. Electrochem. Soc.* **1979**, *126* (12), 2047−2051.
(4) Aurbach, D.; Zinigrad, E.; Cohen, Y.; Teller, H. A Short Review of Failure Mechanisms of Lithium Metal and Lithiated Graphite Anodes in Liquid Electrolyte Solutions. *Solid State Ionics* **2002**, *148* (3), 405−416.
(5) Gireaud, L.; Grugeon, S.; Laruelle, S.; Yrieix, B.; Tarascon, J.-M. Lithium Metal Stripping/Plating Mechanisms Studies: A Metallurgical Approach. *Electrochem. Commun.* **2006**, *8* (10), 1639−1649.
(6) Kim, H.; Jeong, G.; Kim, Y.-U.; Kim, J.-H.; Park, C.-M.; Sohn, H.-J. Metallic Anodes for next Generation Secondary Batteries. *Chem. Soc. Rev.* **2013**, *42* (23), 9011−9034.
(7) Lu, D.; Shao, Y.; Lozano, T.; Bennett, W. D.; Graff, G. L.; Polzin, B.; Zhang, J.; Engelhard, M. H.; Saenz, N. T.; Henderson, W. A.; Bhattacharya, P.; Liu, J.; Xiao, J. Failure Mechanism for Fast-Charged Lithium Metal Batteries with Liquid Electrolytes. *Adv. Energy Mater.* **2015**, *5* (3), 1400993.
(8) Zhang, C.; Liu, S.; Li, G.; Zhang, C.; Liu, X.; Luo, J. Incorporating Ionic Paths into 3D Conducting Scaffolds for High Volumetric and Areal Capacity, High Rate Lithium-Metal Anodes. *Adv. Mater.* **2018**, *30* (33), 1801328.
(9) Liu, Y.; Lin, D.; Yuen, P. Y.; Liu, K.; Xie, J.; Dauskardt, R. H.; Cui, Y. An Artificial Solid Electrolyte Interphase with High Li-Ion Conductivity, Mechanical Strength, and Flexibility for Stable Lithium Metal Anodes. *Adv. Mater.* **2017**, *29* (10), 1605531.
(10) Zhang, J.-G.; Xu, W.; Henderson, W. A. Introduction. *Lithium Metal Anodes and Rechargeable Lithium Metal Batteries*; Springer Series in Materials Science; Springer International: Cham, Switzerland, 2017; Chapter 1, pp 1−4.
(11) Xu, W.; Wang, J.; Ding, F.; Chen, X.; Nasybulin, E.; Zhang, Y.; Zhang, J.-G. Lithium Metal Anodes for Rechargeable Batteries. *Energy Environ. Sci.* **2014**, *7* (2), 513−537.
(12) Hagen, M.; Hanselmann, D.; Ahlbrecht, K.; Maça, R.; Gerber, D.; Tübke, J. Lithium−Sulfur Cells: The Gap between the State-of-the-Art and the Requirements for High Energy Battery Cells. *Adv. Energy Mater.* **2015**, *5* (16), 1401986.
(13) Ossola, F.; Pistoia, G.; Seeber, R.; Ugo, P. Oxidation Potentials of Electrolyte Solutions for Lithium Cells. *Electrochim. Acta* **1988**, *33* (1), 47−50.
(14) Xu, K. Nonaqueous Liquid Electrolytes for Lithium-Based Rechargeable Batteries. *Chem. Rev.* **2004**, *104* (10), 4303−4418.

DOI: 10.1021/acsaem.9b01203
ACS Appl. Energy Mater. 2020, 3, 200−207

(15) Yamada, Y.; Yamada, A. Review—Superconcentrated Electrolytes for Lithium Batteries. *J. Electrochem. Soc.* **2015**, *162* (14), A2406−A2423.
(16) Yamada, Y.; Wang, J.; Ko, S.; Watanabe, E.; Yamada, A. Advances and Issues in Developing Salt-Concentrated Battery Electrolytes. *Nat. Energy* **2019**, *4* (4), 269−280.
(17) Jeong, S.-K.; Seo, H.-Y.; Kim, D.-H.; Han, H.-K.; Kim, J.-G.; Lee, Y. B.; Iriyama, Y.; Abe, T.; Ogumi, Z. Suppression of Dendritic Lithium Formation by Using Concentrated Electrolyte Solutions. *Electrochem. Commun.* **2008**, *10* (4), 635−638.
(18) Qian, J.; Henderson, W. A.; Xu, W.; Bhattacharya, P.; Engelhard, M.; Borodin, O.; Zhang, J.-G. High Rate and Stable Cycling of Lithium Metal Anode. *Nat. Commun.* **2015**, *6*, 6362.
(19) Nie, M.; Abraham, D. P.; Seo, D. M.; Chen, Y.; Bose, A.; Lucht, B. L. Role of Solution Structure in Solid Electrolyte Interphase Formation on Graphite with LiPF6 in Propylene Carbonate. *J. Phys. Chem. C* **2013**, *117* (48), 25381−25389.
(20) Li, Z.; Huang, J.; Yann Liaw, B.; Metzler, V.; Zhang, J. A Review of Lithium Deposition in Lithium-Ion and Lithium Metal Secondary Batteries. *J. Power Sources* **2014**, *254*, 168−182.
(21) Lu, Y.; Tikekar, M.; Mohanty, R.; Hendrickson, K.; Ma, L.; Archer, L. A. Stable Cycling of Lithium Metal Batteries Using High Transference Number Electrolytes. *Adv. Energy Mater.* **2015**, *5* (9), 1402073.
(22) McOwen, D. W.; Seo, D. M.; Borodin, O.; Vatamanu, J.; Boyle, P. D.; Henderson, W. A. Concentrated Electrolytes: Decrypting Electrolyte Properties and Reassessing Al Corrosion Mechanisms. *Energy Environ. Sci.* **2014**, *7* (1), 416−426.
(23) Sharova, V.; Moretti, A.; Diemant, T.; Varzi, A.; Behm, R. J.; Passerini, S. Comparative Study of Imide-Based Li Salts as Electrolyte Additives for Li-Ion Batteries. *J. Power Sources* **2018**, *375*, 43−52.
(24) Kerner, M.; Plylahan, N.; Scheers, J.; Johansson, P. Thermal Stability and Decomposition of Lithium Bis(Fluorosulfonyl)Imide (LiFSI) Salts. *RSC Adv.* **2016**, *6* (28), 23327−23334.
(25) Qiu, F.; Li, X.; Deng, H.; Wang, D.; Mu, X.; He, P.; Zhou, H. A Concentrated Ternary-Salts Electrolyte for High Reversible Li Metal Battery with Slight Excess Li. *Adv. Energy Mater.* **2019**, *9* (6), 1803372.
(26) Beyene, T. T.; Bezabh, H. K.; Weret, M. A.; Hagos, T. M.; Huang, C.-J.; Wang, C.-H.; Su, W.-N.; Dai, H.; Hwang, B.-J. Concentrated Dual-Salt Electrolyte to Stabilize Li Metal and Increase Cycle Life of Anode Free Li-Metal Batteries. *J. Electrochem. Soc.* **2019**, *166* (8), A1501−A1509.
(27) Qian, J.; Adams, B. D.; Zheng, J.; Xu, W.; Henderson, W. A.; Wang, J.; Bowden, M. E.; Xu, S.; Hu, J.; Zhang, J.-G. Anode-Free Rechargeable Lithium Metal Batteries. *Adv. Funct. Mater.* **2016**, *26* (39), 7094−7102.
(28) Zhang, X.; Kostecki, R.; Richardson, T. J.; Pugh, J. K.; Ross, P. N. Electrochemical and Infrared Studies of the Reduction of Organic Carbonates. *J. Electrochem. Soc.* **2001**, *148* (12), A1341−A1345.
(29) Xing, L.; Zheng, X.; Schroeder, M.; Alvarado, J.; von Wald Cresce, A.; Xu, K.; Li, Q.; Li, W. Deciphering the Ethylene Carbonate−Propylene Carbonate Mystery in Li-Ion Batteries. *Acc. Chem. Res.* **2018**, *51* (2), 282−289.
(30) Hayashi, K.; Nemoto, Y.; Tobishima, S.; Yamaki, J. Mixed Solvent Electrolyte for High Voltage Lithium Metal Secondary Cells. *Electrochim. Acta* **1999**, *44* (14), 2337−2344.
(31) Katayama, N.; Kawamura, T.; Baba, Y.; Yamaki, J. Thermal Stability of Propylene Carbonate and Ethylene Carbonate−Propylene Carbonate-Based Electrolytes for Use in Li Cells. *J. Power Sources* **2002**, *109* (2), 321−326.
(32) *1,3-Dioxolane*, MSDS No. 271020; Sigma-Aldrich: Stockholm, Sweden, 2017.
(33) *1,2-Dimethoxyethane*, MSDS No. 259527; Sigma-Aldrich: Stockholm, Sweden, 2019.
(34) *Ethylene Carbonate*, MSDS No. E26258; Sigma-Aldrich: Stockholm, Sweden, 2016.
(35) Bakshi, A. S.; Smith, D. E. Effect of Fat Content and Temperature on Viscosity in Relation to Pumping Requirements of Fluid Milk Products. *J. Dairy Sci.* **1984**, *67* (6), 1157−1160.
(36) Wood, K. N.; Kazyak, E.; Chadwick, A. F.; Chen, K.-H.; Zhang, J.-G.; Thornton, K.; Dasgupta, N. P. Dendrites and Pits: Untangling the Complex Behavior of Lithium Metal Anodes through Operando Video Microscopy. *ACS Cent. Sci.* **2016**, *2* (11), 790−801.
(37) Adams, B. D.; Zheng, J.; Ren, X.; Xu, W.; Zhang, J.-G. Accurate Determination of Coulombic Efficiency for Lithium Metal Anodes and Lithium Metal Batteries. *Adv. Energy Mater.* **2018**, *8* (7), 1702097.
(38) Langenhuizen, N. P. W. The Effect of Mass Transport on Li Deposition and Dissolution. *J. Electrochem. Soc.* **1998**, *145* (9), 3094−3099.
(39) Qian, J.; Xu, W.; Bhattacharya, P.; Engelhard, M.; Henderson, W. A.; Zhang, Y.; Zhang, J.-G. Dendrite-Free Li Deposition Using Trace-Amounts of Water as an Electrolyte Additive. *Nano Energy* **2015**, *15*, 135−144.
(40) Adams, B. D.; Carino, E. V.; Connell, J. G.; Han, K. S.; Cao, R.; Chen, J.; Zheng, J.; Li, Q.; Mueller, K. T.; Henderson, W. A.; Zhang, J.-G. Long Term Stability of Li-S Batteries Using High Concentration Lithium Nitrate Electrolytes. *Nano Energy* **2017**, *40*, 607−617.
(41) Genovese, M.; Louli, A. J.; Weber, R.; Hames, S.; Dahn, J. R. Measuring the Coulombic Efficiency of Lithium Metal Cycling in Anode-Free Lithium Metal Batteries. *J. Electrochem. Soc.* **2018**, *165* (14), A3321−A3325.
(42) Albertus, P.; Babinec, S.; Litzelman, S.; Newman, A. Status and Challenges in Enabling the Lithium Metal Electrode for High-Energy and Low-Cost Rechargeable Batteries. *Nat. Energy* **2018**, *3* (1), 16.
(43) Liu, J.; Bao, Z.; Cui, Y.; Dufek, E. J.; Goodenough, J. B.; Khalifah, P.; Li, Q.; Liaw, B. Y.; Liu, P.; Manthiram, A.; Meng, Y. S.; Subramanian, V. R.; Toney, M. F.; Viswanathan, V. V.; Whittingham, M. S.; Xiao, J.; Xu, W.; Yang, J.; Yang, X.-Q.; Zhang, J.-G. Pathways for Practical High-Energy Long-Cycling Lithium Metal Batteries. *Nat. Energy* **2019**, *4*, 180−186.
(44) Liu, Y.; Lin, D.; Li, Y.; Chen, G.; Pei, A.; Nix, O.; Li, Y.; Cui, Y. Solubility-Mediated Sustained Release Enabling Nitrate Additive in Carbonate Electrolytes for Stable Lithium Metal Anode. *Nat. Commun.* **2018**, *9* (1), 3656.

DOI: 10.1021/acsaem.9b01203
ACS Appl. Energy Mater. 2020, 3, 200−207